ELSEVIER

International Journal of Minerals, Metallurgy and Materials
Volume 16, Number 2, April 2009, Page 189

Materials

Mathematical modeling and simulation of the interface region of a tri-layer composite material, brass-steel-brass, produced by cold rolling

H. Arabi, S.H. Seyedein, A. Mehryab, and B. Tolaminejad

School of Metallurgy and Materials Engineering, Iran University of Science and Technology, IUST, Narmak, Tehran, Iran
(Received 2008-04-17)

Abstract: The object of this study was to find the optimum conditions for the production of a sandwich composite from the sheets of brass-steel-brass. The experimental data obtained during the production process were used to validate the simulation program, which was written to establish the relation between the interface morphology and the thickness reduction amount of the composite. For this purpose, two surfaces of a steel sheet were first prepared by scratching brushing before inserting it between two brass sheets with smooth surfaces. Three sheets were then subjected to a cold rolling process for producing a tri-layer composite with various thicknesses. The sheet interface after rolling was studied by different techniques, and the bonding strength for each rolling condition was determined by peeling test. Moreover, a relation between interfacial bonding strength and thickness reduction was found. The simulation results were compared with the experimental data and the available theoretical models to modify the original simulation program with high application efficiency used for predicting the behavior of the interface under different pressures.

Key words: sandwich composite; cold rolling; mathematical simulation; metallic bonding; interface

Nomenclature:

B: Width of strips;
n: Rotational velocity of the roll, r/min;
R_0: Radius of rolls;
v*: Shear velocity;
α_n: Contact angle related to neutral points;
α_2: Entrance point angle;
U: Linear velocity of the roll;
τ_s: Shear stress;
P: Pressure;
$\overline{\sigma}$: Average stress;
ε^0: Strain rate;
m_1: Friction coefficient between the roll surface and the outer surface of the upper layer;
m_2: Friction coefficient between the roll surface and the outer surface of the underneath layer;
t_{01}: Original thickness of the upper brass layer;
t_{02}: Original thickness of the middle steel layer;
t_{03}: Original thickness of the lower brass layer;
σ_{01}: Yield strength of the upper layer;
σ_{02}: Yield strength of the middle layer;
σ_{03}: Yield strength of the lower layer;
t_{f1}: Final thickness of the upper brass layer;
t_{f2}: Final thickness of the middle steel layer;
t_{f3}: Final thickness of the lower brass layer;
R_t : Reduction percentage of the total thickness.

1. Introduction

Cold roll welding is one of the solid state welding processes that can be used for joining two or more sheet metals by passing them through the gap space of two prefect rolls at ambient temperature. This technique is used in the production of composite sheet materials for various applications [1-3]. The mechanism of joining sheet metals in this process is said [4] to be primary due to metallic bonding between the surface atoms of the sheets. Since this process is performed at room temperature, the effect of rolling pressure on joining sheet metals becomes very crucial as there is no any conventional diffusion at this temperature [5]. In fact, in the cold roll welding process, a certain amount of rolling pressure can cause the atoms within the interface region of sheets to settle in such a way that an equivalent atomic distance to those of sheet metals involved be established at the interface [6]. The preparation of metal sheets before rolling is one of the most important factors for joining. This can be carried out either by coating the surfaces of the harder layer or

Corresponding author: Behzad Tolaminejad, **E-mail:** btolaminejad@iust.ac.ir
Also available online at www.sciencedirect.com

by scratch brushing its surfaces [7-10]. In the scratch brushing method, asperities (*i.e.* scratches consisted of peaks and troughs) are produced during brushing the surface. The peaks undergo the maximum deformation during rolling; hence, it becomes harder and subsequently some microcracks appear in the surfaces. The surfaces of these microcracks consist of virgin metals (*i.e.* non-oxide surfaces), so when they come in contact with the softer metal extruded through microcracks during cold rolling, some metallic bonds can be established between the two metals [3, 8].

2. Experimental work

Before the application of cold rolling process in the present work, the surfaces of steel cores of the three-layer composite, brass-steel-brass were prepared by the scratch brushing technique. Then a sheet of brass with smooth surfaces was put over each side of the brushed steel sheet before rolling the three sheets at room temperature. Different thickness reductions (R_t=12%-71%) were applied to investigate the effect of rolling pressure on bonding strength and to find the optimum pressure for the production of the composite with enough bonding strength suitable for the next stage of operation, which was deep drawing after the annealing stage. The details of material compositions, the joining operation, and the peeling test for the evaluation of bonding strength can be found else where [11-12]. However, in this article, the mechanism of locking at the interface region has been simulated adequately, so that it can properly justify the relation between the observed microstructural changes during rolling and the pressure used for the cold welding process. To make these ends meet, the pressures applied for a certain amount of thickness reduction were established from the laboratory data, and then by use of Ansys-7.1 software, the variation of interface morphology for different thickness reductions was estimated. Finally, the relation between the bonding strength of the interface and thickness reduction was established, and an efficient mathematical model for this relationship was proposed.

3. Theoretical work

3.1. Calculation of pressure by the upper bound theorem

The upper bound theorem for the calculation of the required pressure for a certain amount of thickness reduction was used in the following way. According to Ref. [13], the total power by the outer force=the internal power for heterogeneous deformation + the required power for ideal deformation.

$$PU = \sigma_{\text{avr}} AU \leq \int_v \bar{\sigma}\ \varepsilon^0 \mathrm{d}v + \int_s \tau_s \upsilon^* \mathrm{d}s \tag{1}$$

where P is the upper bound force or the roll separating load. This force is higher than the actual force required for deformation and is a function of rolling variables. By minimizing this equation on the base of independent variables, the predicted required force can come near to the actual force.

(1) Calculation of power.

Fig. 1 shows a schematically deformation pattern produced during the rolling of sandwich layers. The calculation of power for rolling three layers, that is the estimated upper bound power required for the deformation (J) of the three layers, was determined by using Eq.(1) in the following way [14-15]. The total required power during rolling according to the upper bound theorem can be expressed as

$$J = W_{\text{it}} + W_{\text{st}} + W_{\text{sf}} \tag{2}$$

where, W_{it}, W_{st}, and W_{sf} are the internal power dissipated during the process, the shear power due to velocity discontinuity in neighboring fields, and the shear power losses due to the friction between brass sheets and rolls, respectively. The detailed expressions of the individual terms in Eq. (2) are as follows.

(a) Internal ideal power (W_{it}) of deformation:

$$W_{\text{it}} = \frac{2b}{\sqrt{3}} U \cdot \frac{\dfrac{t_{\text{f1}} + t_{\text{f2}} + t_{\text{f3}}}{R_0} + \alpha_n^2}{\dfrac{t_{\text{f1}} + t_{\text{f2}} + t_{\text{f3}}}{R_0}} \cdot \left[\sigma_{01} t_{\text{f1}} \cdot \ln \frac{t_{01}}{t_{\text{f1}}} + \sigma_{02} t_{\text{f2}} \cdot \ln \frac{t_{02}}{t_{\text{f2}}} + \sigma_{03} t_{\text{f3}} \cdot \ln \frac{t_{03}}{t_{\text{f3}}} \right] \tag{3}$$

(b) Shear power (W_{st}) due to the velocity discontinuity in neighboring fields:

$$W_{\text{st}} = bU \left(1 + \frac{R_0}{t_{\text{f1}} + t_{\text{f2}} + t_{\text{f3}}} \alpha_n^2 \right) \cdot \frac{(t_{\text{f1}} + t_{\text{f2}} + t_{\text{f3}})^{\frac{3}{2}} \sqrt{\dfrac{t_{01} + t_{02} + t_{03}}{t_{\text{f1}} + t_{\text{f2}} + t_{\text{f3}}} - 1}}{(t_{01} + t_{02} + t_{03})^2 \sqrt{R_0}} \cdot \left\{ \frac{\sigma_{01}}{\sqrt{3}} (t_{02} + t_{03}) \cdot t_{01} + \frac{\sigma_{02}}{4\sqrt{3}} \left[(t_{02} + t_{03} - t_1)^2 + (t_{01} + t_{02} - t_{03})^2 \right] + \frac{\sigma_{03}}{\sqrt{3}} \cdot t_{03} (t_{01} + t_{02}) \right\} \tag{4}$$

(c) Shear power losses (W_{sf}) due to the friction between brass sheets and rolls:

$$W_{\mathrm{sf1}} = bUR_0 \frac{m_1\sigma_{01}}{\sqrt{3}} \cdot \left\{ 2\tan^{-1}\left[\alpha_n \sqrt{R_0/(t_{\mathrm{f1}}+t_{\mathrm{f2}}+t_{\mathrm{f3}})} \right] - \tan^{-1}\sqrt{\frac{t_{01}+t_{02}+t_{03}}{t_{\mathrm{f1}}+t_{\mathrm{f2}}+t_{\mathrm{f3}}}} \right\} \cdot \left[\left(1+\frac{R_0\alpha_n^2}{t_{\mathrm{f1}}+t_{\mathrm{f2}}+t_{\mathrm{f3}}} \right) \sqrt{\frac{t_{\mathrm{f1}}+t_{\mathrm{f2}}+t_{\mathrm{f3}}}{R_0}} + (\alpha_2 - 2\alpha_n) \right] \tag{5}$$

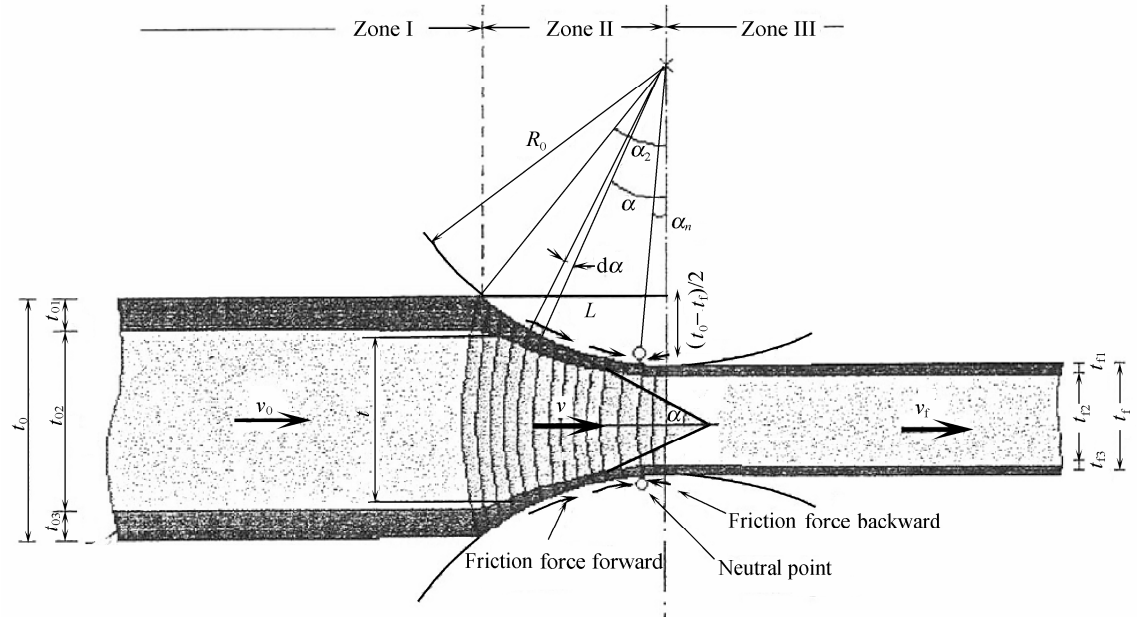

Fig. 1. Schematic of the deformation pattern, and the significant of the symbols used.

The symbols used in the above formula are defined in nomenclature, and the significance of some of these symbols is shown in Fig. 1. The total shear power losses due to the friction between sheet composite surfaces and rolls are determined by the sum of W_{sf1} and W_{sf2}.

$$W_{\mathrm{sf}}=W_{\mathrm{sf1}}+W_{\mathrm{sf2}} \tag{6}$$

$$J= W_{\mathrm{it}}+W_{\mathrm{st}}+W_{\mathrm{sf}} \tag{7}$$

$$J = \left[\frac{2b}{\sqrt{3}} U \cdot \frac{\frac{t_{\mathrm{f1}}+t_{\mathrm{f2}}+t_{\mathrm{f3}}}{R_0}+\alpha_n^2}{\frac{t_{\mathrm{f1}}+t_{\mathrm{f2}}+t_{\mathrm{f3}}}{R_0}} \cdot \left(\sigma_{01}t_{\mathrm{f1}} \cdot \ln\frac{t_{01}}{t_{\mathrm{f1}}} + \sigma_{02}t_{\mathrm{f2}} \cdot \ln\frac{t_{02}}{t_{\mathrm{f2}}} + \sigma_{03}t_{\mathrm{f3}} \cdot \ln\frac{t_{03}}{t_{\mathrm{f3}}} \right) \right] + bU\left(1+\frac{R_0}{t_{\mathrm{f1}}+t_{\mathrm{f2}}+t_{\mathrm{f3}}} \cdot \alpha_n^2 \right) \times$$

$$\frac{(t_{\mathrm{f1}}+t_{\mathrm{f2}}+t_{\mathrm{f3}})^{\frac{3}{2}} \sqrt{\frac{t_{01}+t_{02}+t_{03}}{t_{\mathrm{f1}}+t_{\mathrm{f2}}+t_{\mathrm{f3}}}-1}}{(t_{01}+t_{02}+t_{03})^2\sqrt{R_0}} \times$$

$$\left\{ \frac{\sigma_{01}}{\sqrt{3}}(t_{02}+t_{03}+t_{03})t_{01} + \frac{\sigma_{02}}{4\sqrt{3}}\left[(t_{02}+t_{03}-t_{01})^2 + (t_{01}+t_{02}-t_{03})^2 \right] + \frac{\sigma_{01}}{\sqrt{3}} t_{03}(t_{01}+t_{02}) \right\} +$$

$$bUR_0 \cdot \frac{(m_1\sigma_{01}+m_2\sigma_{03}}{\sqrt{3}} \times$$

$$\left[\left(2\tan^{-1}\alpha_n\sqrt{R_0/(t_{\mathrm{f1}}+t_{\mathrm{f2}}+t_{\mathrm{f3}})} - \tan^{-1}\sqrt{\frac{t_{01}+t_{02}+t_{03}}{t_{\mathrm{f1}}+t_{\mathrm{f2}}+t_{\mathrm{f3}}}-1} \right) \left(1+\frac{R_0\alpha_n^2}{t_{\mathrm{f1}}+t_{\mathrm{f2}}+t_{\mathrm{f3}}} \right) \sqrt{\frac{t_{\mathrm{f1}}+t_{\mathrm{f2}}+t_{\mathrm{f3}}}{R_0}} + (\alpha_2-2\alpha_n) \right] \tag{8}$$

This equation is the most suitable equation for the calculation of the required power for a certain thickness reduction in a three-layer composite under different variants such as initial sheet thickness, roller diameter, friction conditions, and so on.

(2) Calculation of rolling pressure and torque.

Rolling pressure was calculated from the required power for rolling or compression power (*i.e. J*) according to the published relationship in Refs. [16-17].

$$P = \frac{J}{4\pi aN} = \frac{J}{4\pi N \cdot \lambda[R(t_0-t_{\mathrm{F}})]^{1/2}} \tag{9}$$

where coefficient λ for cold rolling sheets having

smooth surfaces is said to be equal to [14]:

$$\lambda = \frac{a}{LP} = \frac{a}{[R(t_0 - t_F)]^{1/2}} \approx 0.48 \quad (10)$$

where a is the tangential radius that rolling load is supposed to be controlled or in other words, it is the effective momentum arm as shown in Fig. 2.

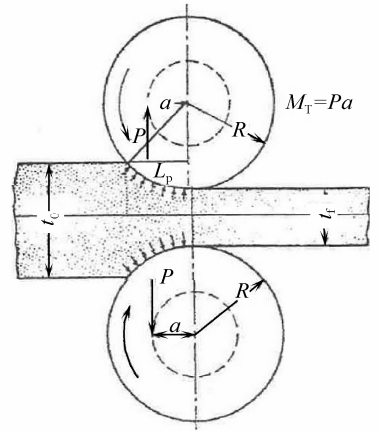

Fig. 2. Effective momentum arm and the point that the load is supposed to be concentrated.

3.2. Computational modeling

(1) Flowchart of computational study.

A computer program on the base of the upper bound theorem was used for minimizing the power and also calculating the rolling load for a certain amount of reduction in accordance with Eq. (4). The program flowchart is presented in Fig. 3.

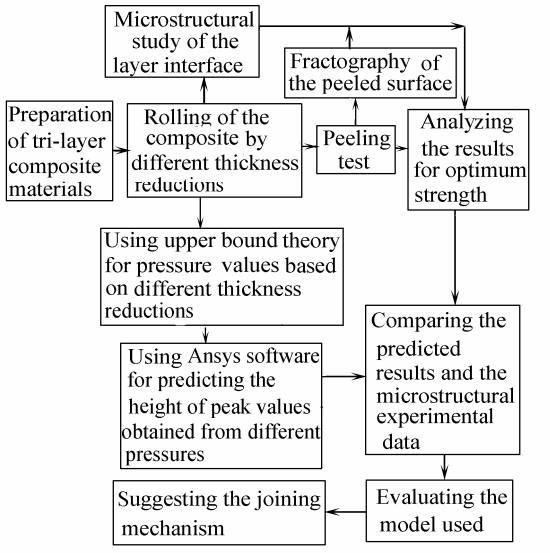

Fig. 3. Flowchart of the theoretical study and practical work used for modeling.

The primary conditions used in this program are as follows.

The angle, α_n, was chosen between zero (*i.e.*, normal to the rolling direction) and α_2 (*i.e.* $0<\alpha_n<\alpha_2$), where α_2 is the entrance point angle. Moreover, the program was written in such a way that the range of thickness reduction (R_t) was chosen between 12% and 71%.

$$t_f=t_0(1-R_t),$$

$$t_0=t_{01}+t_{02}+t_{03} \quad (11)$$

This range of R_t covers all the thickness reductions used in this research. By estimating the final reduction and the angle α_n via the program during the minimization process, the rolling pressure for any specific reduction was predicted.

(2) Simulation of the interface region.

The finite element method (FEM) through Ansys 7.1 software was used for simulating the interface morphology and the required pressure. The total thickness of the sheet composite was 4.4 mm. Half of the total thickness is shown schematically in Fig. 4. Two different types of steels for the middle layer of the sandwich were used. The specification of the materials is presented in Table 1.

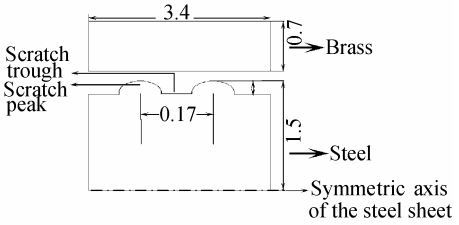

Fig. 4. Schematic model for the interface simulation (unit: mm).

After producing the three sheet brass-steel-brass composites under various thickness reductions, the interfaces of steel and brass layers were studied by use of optical and scanning electron microscopes. The size, shape, and height of the compressed peaks of scratch brushes in optimum conditions were investigated and the results were compared with those computed with the mathematical model through the simulating program. The schematic mesh size used in this study for modeling the interface region on one side of the symmetric axis is shown in Fig. 5.

4. Results and discussion

The simulation process for different rolling pressures under various thickness reductions lead to the variation of the steel-brass interface bonding strength presented in Fig. 6. Meanwhile, the rolling pressure, which was calculated by the upper bound theorem, increases as the thickness reduction increases. The changes in the shapes of scratch peaks as they subjected to various rolling pressures are illustrated in Fig.7.

Figs. 7(a)-(e) show that the height of the peaks re-

duces as the rolling pressure (computed by the proposed relation, *i.e*. Eq. (4)) increases. It is mentioned earlier that as the heights of the peaks decrease, the material underneath becomes harder. This situation continues until further hardening of the material becomes practically impossible, which then forms extrusion channels or microcracks for the upper soft material (Fig. 7(f)). The extruded brass within the microcracks is termed as micropins regions. The details of the effect of micropins on the strengthening mechanism of the interface have been published earlier [11-12].

Table 1. Specification of the material for sandwich sheet composites

Position	Material	Poisson's ratio	Young's modulus / GPa	Yield strength / MPa
Middle layer	St13	0.29	205	285
Lower & upper layers	CuZn10	0.32	120	125
Micropins region	Work hardened St13	0.29	205	620*

Note: * was obtained from the microhardness data after rolling.

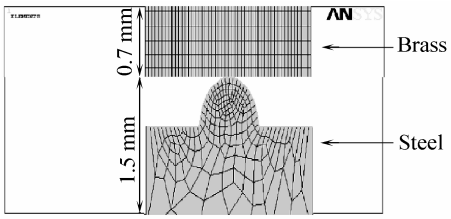

Fig. 5. Schematic illustration of meshing in an interface region

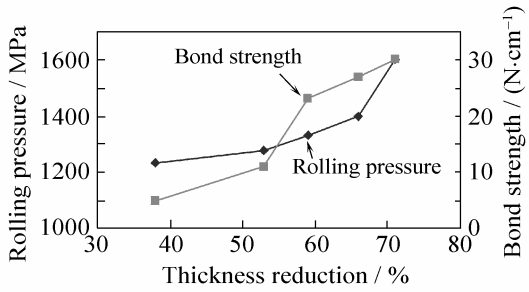

Fig. 6. Calculated rolling pressure and bonding strength *vs.* thickness reduction (calculated by the upper bound theorem).

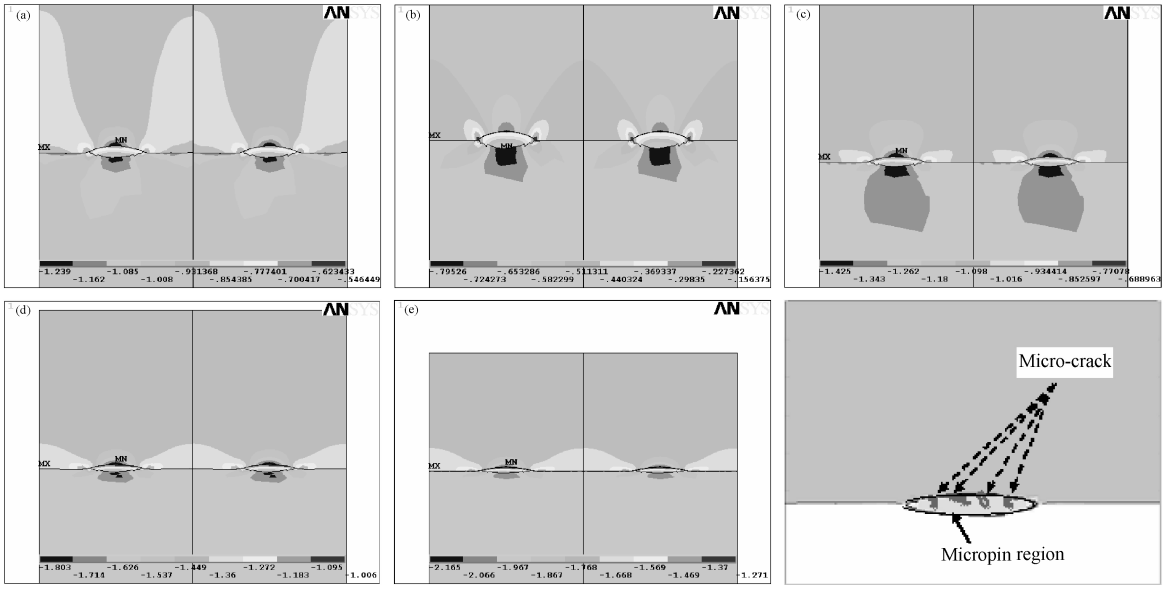

Fig. 7. Variation of strain induced in the thickness direction of layers imposed by different R_t: (a) 38%; (b) 52%; (c) 59%; (d) 66%; (e) 71%; (f) schematic illustration of microcrack formation on the hardened peak region of scratches.

Fig. 8 shows that the peak regions are compressed and deform severely so that their hardness increases subsequently, see Table 2. The peeled surface of the steel sheet is presented in Fig. 8(b) and the X-ray photograph of copper element on this sheet after the peeling test is shown in Fig.8(c). The trace of copper element on the steel sheet surface between the troughs confirms the penetration of copper element within the microcracks produced in the hardened peak regions during rolling.

Fig. 9 shows the amount of reduction occurred on the peak heights when the composite thickness reduced more. It indicates that after the application of a large amounts of thickness reductions (*i.e.* >66%), the interface of brass-steel sheets approximately levels off. However, since the bonding mechanism of these sheets is mostly due to the formation of micropins and the metallic bonding within them [11-12], one can expect that the strain field in the vicinity of the interface be heterogeneously distributed as shown in Fig. 7.

Stress concentration around the peak regions is much more than that concentrated on the trough regions.

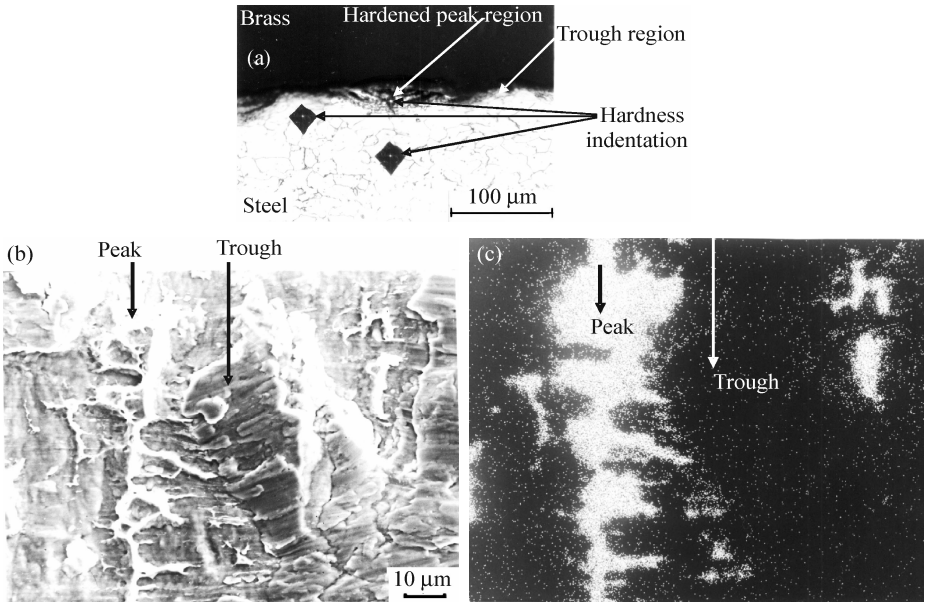

Fig. 8. Typical profile of the sheet composite after rolling (a), peeled surface of the steel sheet (b), and X-ray map of copper element taken from the peeled surface of the steel sheet (c), showing the penetration of softer material (*i.e.*, brass) within the hardened peak regions of the steel sheet.

Table 2. Hardness of various locations of the steel sheet before and after rolling process

Location	Trough	Peak	Central region
Hardness of the original scratch brushed steel, Hv_{20}	110	200	90
Hardness of the 59% reduction steel, Hv_{20}	187	327	160

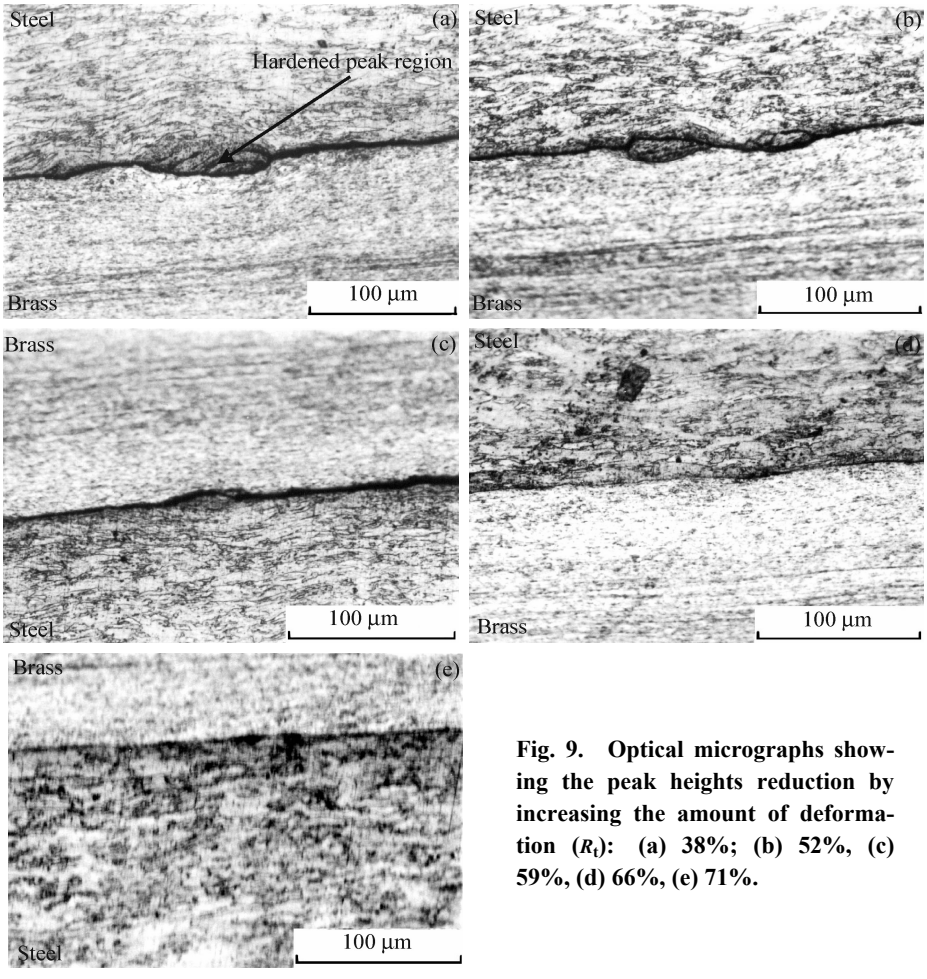

Fig. 9. Optical micrographs showing the peak heights reduction by increasing the amount of deformation (R_t): (a) 38%; (b) 52%, (c) 59%, (d) 66%, (e) 71%.

By comparing Figs. 7 and 9 for actual reduction of the height of peaks with the increase in the amount of thickness reduction, one can conclude that the simulated program used in this research was in a good agreement with the experimental data obtained during the rolling process. The height of peaks estimated from the mathematical model and those calculated from the experimental data for different amounts of deformations as a function of total thickness reduction is presented in Fig. 10. It indicates that the height of the peaks obtained experimentally does not change critically after 59% of thickness reduction, whereas the heights predicted by the model reduce even after this percentage of thickness reduction. The reason of this observation can be sought in the application of the linear elastic-plastic theory in the model for the entire thickness reduction range. Whereas deformation in the peaks of scratches in the steel sheet is actually logarithmic; the trend of reduction estimated by the model is linear and very close to the data obtained experimentally. Fig. 11 also illustrates the differences between the linear work hardening and true stress-strain diagram for the plastic region in a deformation process [15].

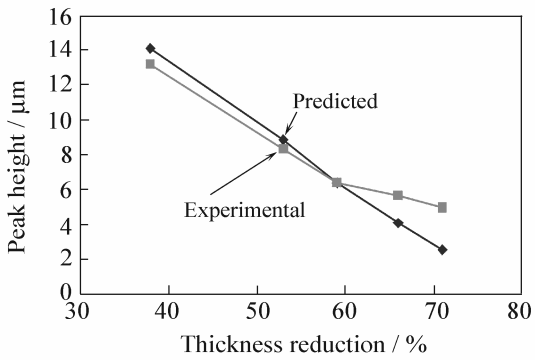

Fig. 10. Comparison of the predicted and experimental heights of the peaks for various thickness reductions.

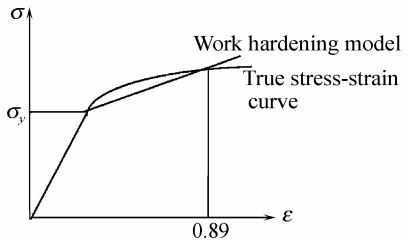

Fig. 11. Comparison between the linear and logarithmic work hardening models [14].

The work hardening rate of the steel predicted by theory is usually less than the actual hardening rate up to a certain amount of reduction as indicated in Fig. 11. This specific amount of reduction is about 59% for this research as indicated in Fig. 10. The peaks of scratches initially deform at a higher rate as the material is soft and the dislocations can be generated and move easily, but the amount of deformation reduces gradually to a minimum as the material becomes harder. The theoretical peak heights are smaller than those produced experimentally up to 59% as indicated Fig. 10. Thereafter, the hardness of experimentally peaks is less than those produced by theory. Indeed, for a thickness reduction more than 59%, nearly full strength of the material has been reached, so that the material under peak regions becomes fully hardened and no more deformation can be applied until the material is subjected to thermal treatment. The spherical shape of peak regions becomes elliptical after rolling. So the model predicts the shape of peak regions is in good agreement with the experimental results. Furthermore, the comparison of peak regions for a thickness reduction of 59% for both theoretical and experimental results show that the predicted rolling pressure can be credited for use in the cold welding process. It is worth emphasizing that the dominant bonding mechanism is independent of the trough region morphology changes and just relates to the extremity limitation of micropins creations. Also, the interface strength of the layers can be predicted from the theoretical peak heights estimated from the computer program used in this work.

5. Conclusions

(1) The optimum thickness reduction estimated by the upper bound theorem and also obtained experimentally for the cold roll welding of brass-steel-brass sheet composites was 59%.

(2) During the rolling, with brass flowing in the trough regions of the steel sheet, mechanical locking was initially created prior to the threshold thickness reduction of 38%. However, the main mechanism of interface strengthening occurred when the soft brass extruded within the microcracks separated on the hardened peak regions during further reduction.

(3) Peaks of scratches reduce linearly with increasing reduction amount; however, the reduction rate up to 59% is higher than that of further reduction.

(4) The good agreement between the theoretical peak height values obtained by simulation and the empirical model developed in this work makes the predicted values of rolling pressure for any specific reduction credited.

References

[1] N. Bay, Cold welding part II—process variation and applications, *Met. Constr.*, 18(1986), p.486.

[2] J.A. Forster and A. Amatruda, The processing and evaluation of clad metals, *JOM*, 45(1993), No.6, p.35.

[3] R.L. Brien, Cold welding, *Welding Handbook*, American Welding Society for Metals, 12(1991), p.814.

[4] International Organization, ISO R 857, *Standard of Welding Terms*, National Institute of Standards and Technology, 2004.

[5] K. Thomas and M. Petri, Cold welding, *ASM Handbook*, American Welding Society for Metals, 6(1994), p.312.

[6] S.H. Avener, *Introduction to Physical Metallurgy*, McGraw-Hill, Auckland, 1974, p.79.

[7] R.F. Tylcote, Investigation on pressure welding, *Br. Weld. J.*, 5(1994), p.117.

[8] R. Dixon, Introduction to solid state welding, *ASM Metals Handbook*, 6(1989), p.140.

[9] B. Tolaminejad and H. Arabi, A study of roll-bonding MS90 alloy to steel utilizing chromized interlayer, *Iranian J. Sci. Technol.,* 32(2008), p.631.

[10] B. Tolaminejad, A. Karimi Taheri, H. Arabi, and M. Shahmiri, An investigation into the effect of ECAE process on the mechanical and microstructural properties of middle layer in aluminum/copper/aluminum laminated composite, [in] *Proceedings of the 4th Metals and Materials Forming MATFORM'87*, Tehran, 2008, p.90.

[11] A. Mehryab, *An Investigation into the Effective Parameters on the Interface Bonding of Brass/Steel/Brass Tri-layer Composite* [Dissertation], Iran University of Science & Technology, Narmak, Tehran, 2005.

[12] A. Mehryab, H. Arabi, M. Tamizifar, and S.H. Seyedein, Study of joining mechanism in brass/steel/brass sandwich materials prepared by scratch brushing method, *Iranian J. Mater. Sci. Eng*., 2(2005), No.1, p.33.

[13] B. Avitzur, *Metal Forming: Processes and Analysis*, McGraw-Hill, Auckland, 1968.

[14] P.G. Hodge, *Plastic Analysis of Structures*, McGraw-Hill, Auckland, 1959, p.283.

[15] W. Prager, *An Introduction to Plasticity*, Addison Wesely, 1959, p.375.

[16] G.E. Dieter, *Mechanical Metallurgy*, 3rd ed., McGraw-Hill, Auckland, 1979.

[17] A.W. Ruff and L.K. Ives, Fundamental of friction and wear of materials, *ASM Int.*, 18(1981), p.235.